Available online at www.cuijca.com

INTERNATIONAL JOURNAL OF COMPUTATIONAL ANALYSIS

Vol (4), No. (1), pp. 18-35

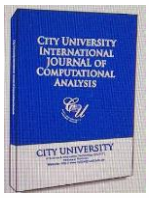

Dynamics of Fractional Order SIR Model with a Case Study of COVID-19 in Turkey

*Zubair Ahmad**[1], Naveed Khan[1], Muhammad Arif[1], Saqib Murtaza[1], and Ilyas Khan[2]*

[1]*Department of Mathematics, City University of Science and Information Technology, Peshawar, 25000 Khyber Pakhtunkhwa, Pakistan.*

[2]*Department of Mathematics, College of Science Al-Zulfi, Majmaah University, Al-Majmaah 11952, Saudi Arabia.*

Keywords:

COVID-19

SEIR model

AB fractional model

Stability Analysis

Real data

Numerical results

A B S T R A C T

The new coronavirus illness 2019 (COVID-19) poses a major danger to civilization today. Despite its simplicity, the susceptible-infected-recovered/removed (SIR) model and its variations are frequently used to predict the spread of COVID 19 across the world. However, using the SIR model to obtain exact solutions is difficult, especially in the early stages of a pandemic when data is few and sometimes noisy. The goal of this study is to describe COVID-19 dynamics in Turkey. The classical model is fractionalized via Atangana-Baleanu fractional derivative. From the 30th of October to the 8th of November 2020, we examine the available infection cases and fit or estimate various parameters appropriately. The basic reproduction number has been obtained as $\Re_0 \approx 1.09457$. To analyse the model's dynamics and transmission, stability analysis is performed at disease free equilibrium DFE and endemic equilibrium EE. Finally, the numerical results of AB fractional model are obtained and the influence of different parameters like fractional parameter γ , contact rate μ , and recovery rate κ on the model are shown by plotting graphs. We have forecasted the disease's spread for the next 800 days.

1 Introduction

Three zoonotic coronaviruses–Severe Acute Respiratory Syndrome (SARS), Middle East Respiratory Syndrome (MERS), and Swine Acute Diarrhoea Syndrome (SADS)–have been linked to large-scale illness outbreaks in the last two decades. COVID-19, a fatal viral illness that initially appeared in Wuhan, Hubei Province, China, in December 2019, has already spread to over 200 countries throughout the world, generating a global emergency. COVID-19 stands for Coronavirus 2 of the Severe Acute Respiratory Syndrome (SARS-CoV-2) [1]. The World Health Organization (WHO) has designated it a worldwide public health emergency [2]. This disease is mostly spread from person to person by direct contact with respiratory droplets, as well as indirectly through fomites in the affected individual's immediate environment [3,4]. Fever, tiredness, dry cough, and myalgia are the most frequent

**Corresponding Author: Zubair Ahmad. Email:* xubair5383@gmail.com

symptoms of COVID-19, however some patients also have headaches, stomach pains, diarrhoea, nausea, and vomiting. Clinical findings reveal that, depending on the immune system, the patient gets morbid within 1-2 days of acute sickness, becomes morbid after 4-6 days, and the infection clears in 18 days [5]. It is reported that the COVID-19's fatality rate is near about 3.4% [6]. There are already quite a few different models of COVID-19 developed and published that have analysed various aspects of disease dynamics and possible containment.

The objective of using mathematical models to investigate infectious diseases is to gain a better understanding of how they spread in a community and to identify some potential solutions for controlling their spread. As a result, in many nations and among other health authorities, mathematical modelling techniques provide strong tools for epidemiological policy decision-making. These models are sometimes the only feasible method for determining which preventative or control method is the most successful. Despite its simplicity, the SIR model and its variations are frequently utilized to forecast the progression of COVID-19 across the world. However, estimating the SIR model with accuracy is difficult, especially in the early phases of a pandemic with limited and sometimes noisy data [7-10].

Fractional order modelling is the generalization of classical models that can explain the dynamical systems more precisely. In the literature, many researchers reported their investigations in different research areas by using other fractional operators such as geotechnical engineering, nanotechnology, heat transfer phenomena, blood flow, cancer therapy, drug delivery, and biochemical reactions [11-14]. Besides this, a lot of research is reported to study the spread of different infections. The transmission of COVID-19 has recently been studied by a number of researchers employing various fractional operators [15]-[17]. Rajagopal et al. [15] used the fractional SEIRD model to investigate the propagation of COVID-19 and found that the fractional order model gives the best crossover behaviour which is more realistic as compared to the classical one. Alkahtani and Alzaid [16] discussed the dynamics of novel coronavirus in Italy. They modelled their problem in terms of non-linear ODE's and fractionalized them by using different operators. Yadav and Verma [17] reported their investigations based on the COVID-19's spread by using CF fractional derivative.

Using the SIR model, we focused at the dynamics of COVID-19 in this work. Initially, we modelled the dynamical system in terms of a system of non-linear ODE's. Furthermore, we fractionalized our integer order model by using the AB-fractional operator. The AB time-fractional derivative was chosen due to non locality and non-sigularity in its kernel that allows it to forecast COVID-19 spread more precisely. Most researchers has chosen the AB fractional model for investigating the forecast of a variety of illness, concluding that the AB fractional derivative yields more accurate results than other fractional operators [18-19]. Qureshi and Yusuf [18] presented an MSEIR model to analyse the transmission of Chickenpox illness using various fractional operators, and found that the AB fractional model delivers more precise results with real data and has a higher efficiency rate than other operators. Qureshi and Atangana [19] studied the spread of dengue fever with the real data of Cape Verde islands using different fractional operators. Many researchers described their investigations for the COVID-19's dynamics using different epidemiological models by considering AB fractional operators such as Abdo *et al.* [20] presented the solutions of a non-linear AB fractional model for the COVID-19's spread through Adams-Bashforth numerical scheme. Similarly, Ahmad et al. [21] predicted the COVID-19's spread in Pakistan by using AB-fractional SEIR model. Other applications of AB fractional derivative can be seen in fluid flow problems, prey-predator models, solar energy and heat transfer phenomena [22-26].

Motivated from the above literature, the present study describes COVID-19's dynamics in Turkey by using SIR model. Initially, we modelled the present epidemiological problem in the form of three non-linear ordinary differential equations with classical order derivative. Then we generalized the integer order model into the fractional model by using AB fractional operator. Positivity and boundedness are shown for the present model. The basic reproduction numbers and equilibrium points are established. Stability analysis is also presented for disease-free and endemic equilibria. In the present study, we have considered the public reported data in the time interval of 10 days i.e. from 30th October 2020 to 8th November 2020, and parameterized the given model for classical order with available data. For the provided fractional model, a numerical approach is constructed and the results for the fractional parameter are analysed. For global asymptotical stability, certain figures are displayed with varied initial conditions.

1. Mathematical Modelling

The propagation of COVID-19 in the human population is examined in this study. The overall population is symbolized by $N(t)$ which contains three different compartments i.e., susceptible, infected, and recovered/removed individuals and are represented with $S(t), I(t)$ and $R(t)$ respectively. Figure 1 shows the contact between these subgroups:

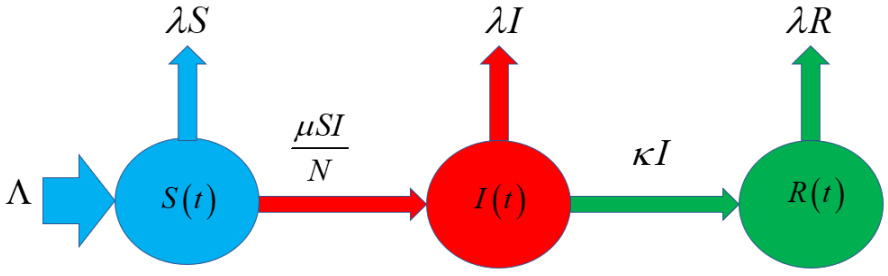

Figure 1. Flow chart of the model.

In this model, Λ is the birth/recruitment rate in the susceptible class, λ represents the death rate, μ is the interaction rate among infected and susceptible species with the route $\frac{\mu SI}{N}$, and κ is the removal/recovery rate of infected individuals. The mathematical form of the considered model can be written as:

$$\left.\begin{aligned}\frac{dS(t)}{dt} &= \Lambda - \lambda S - \frac{\mu SI}{N},\\ \frac{dI(t)}{dt} &= \frac{\mu SI}{N} - \lambda I - \kappa I,\\ \frac{dR(t)}{dt} &= \kappa I - \lambda R,\end{aligned}\right\} \tag{1}$$

Corresponding non-negative ICs

$$S(0) = S^0 \geq 0 \ , \ I(0) = I^0 \geq 0 \text{ and } R(0) = R^0 \geq 0. \tag{2}$$

2. Basic Reproduction Number

Take a look at the second Eq. of system (1):

$$\frac{dI(t)}{dt} = \frac{\mu SI}{N} - \lambda I - \kappa I,$$

$$\Rightarrow \frac{dI(t)}{dt} = \left(\frac{\mu S}{N} - \lambda - \kappa\right) I,$$

$$\Rightarrow \frac{dI(t)}{dt} = (\lambda + \kappa)\left(\frac{\mu S}{N(\lambda + \kappa)} - 1\right) I,$$

$$\Rightarrow \frac{dI(t)}{dt} = (\lambda + \kappa)(\Re_0 - 1) I, \tag{3}$$

Here

$$\Re_0 = \frac{\mu S^0}{\left(S^0 + I^0 + R^0\right)(\lambda + \kappa)} \tag{4}$$

By putting disease free equilibrium here, we get:

$$\Re_0 = \frac{\mu}{(\lambda + \kappa)} \tag{5}$$

3. Equilibrium points

The two possible equilibrium points of model (1) at disease free (DFE) and endemic equilibrium are shown in this section (EE). Let's begin with:

$$\left.\frac{dS(t)}{dt} = \frac{dI(t)}{dt} = \frac{dR(t)}{dt} = 0,\right\} \tag{6}$$

Using equation (6), model (1) becomes:

$$\left.\begin{aligned} 0 &= \Lambda - \lambda S - \frac{\mu SI}{N}, \\ 0 &= \frac{\mu SI}{N} - \lambda I - \kappa I, \\ 0 &= \kappa I - \lambda R, \end{aligned}\right\} \tag{7}$$

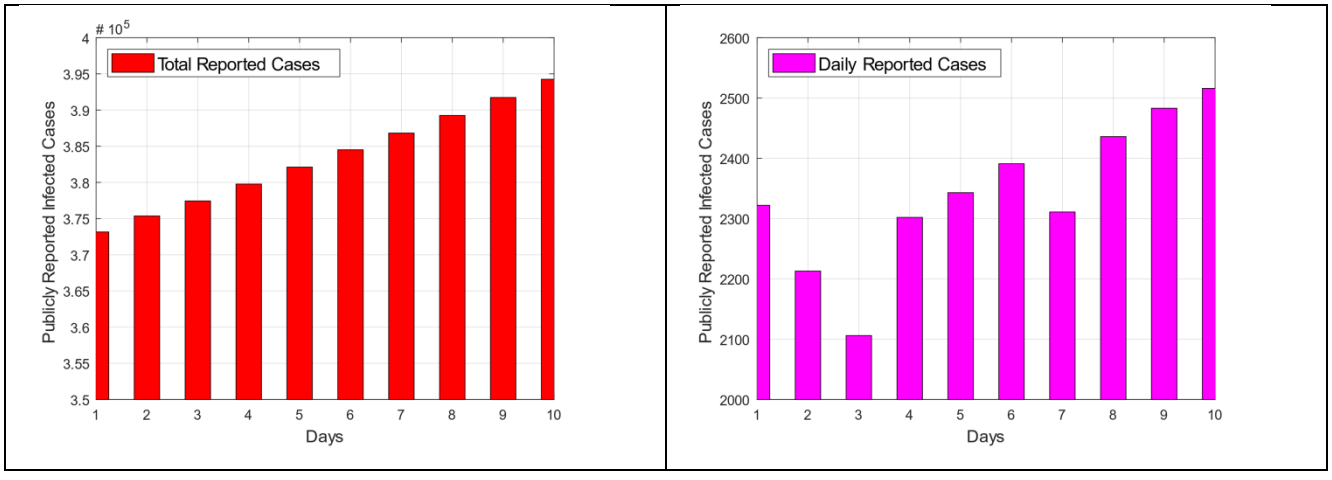

Figure 2. Infection cases of COVID-19 between 30th October 2020 and 8th November 2020.

From equation (7), the possible DFE is given as:

$$\Psi_{DFE} = \left(S^0, I^0, R^0\right) = \left(\frac{\Lambda}{\lambda}, 0, 0\right). \tag{8}$$

Similarly, the EE of model (1) is calculated as:

$$\Psi_{EE} = \left(S^*, I^*, R^*\right) = \left(\frac{\Lambda\left(\lambda+\kappa\right)\Re_0}{\lambda\left(\lambda\Re_0+\kappa\Re_0+\mu-1\right)}, \frac{\Lambda\left(\Re_0-1\right)\Re_0}{\left(\lambda\Re_0+\kappa\Re_0+\mu-1\right)}, \frac{\kappa\Lambda\left(\Re_0-1\right)\Re_0}{\lambda\left(\lambda\Re_0+\kappa\Re_0+\mu-1\right)}\right), \tag{9}$$

4. Stability Analysis

Theorem 4.1. *If* $\Re_0 < 1$, *The DFE* Ψ_{DFE} *of the system* (1) *is locally asymptotically stable.*

Proof: At DFE, system (1)'s Jacobian matrix can be written as:

$$J_{\Psi_{DFE}} = \begin{bmatrix} -\lambda & -\mu & 0 \\ 0 & -\left(\mu-\lambda-\kappa\right) & 0 \\ 0 & \kappa & -\lambda \end{bmatrix} \tag{10}$$

Suppose ℓ denotes the eigenvalues of the Jacobian matrix J_{Ψ^0}. In this situation, the two negative eigenvalues of the aforementioned matrix, i.e. $-\lambda$ (twice). The following characteristic equation can obtain the remaining required eigen values:

$$\ell_3 = \left(\kappa+\lambda\right)\left(\Re_0-1\right)$$

.

From equation (11), it can be noticed that $\kappa, \lambda > 0$. When $\Re_0 < 1$. As a result, the characteristics equation's coefficients are all non-negative. Furthermore, the eigenvalues of the aforementioned characteristic equation are negative according to Rough-Hurtwiz criterion. Thus, all the eigenvalues of the Jacobian matrix (10) are negative for $\Re_0 < 1$. As a result, when $\Re_0 < 1$, the model (1) is locally asymptotically stable.

5. Non-negativity and Boundedness of the Model

The following lemma is used to demonstrate the model's positivity:

Lemma 3.1. *Suppose* $\Phi \subset \mathbb{R}\times\mathbb{C}^n$ *is open,* $f_i \in \mathbb{C}\left(\Phi\mathbb{R}\right)$ *,*$i = 1$ *,* 2 *,* *If* $f_i\big|_{X_i(\tau)=0, X_\tau\in\mathbb{C}^n_{+0}} \geq 0$ $X_\tau = \left(x_{1\tau}, x_{2\tau}, ..., x_{n\tau}\right)^T, i = 1, 2, ..., n$, then $\mathbb{C}^n_{+0}\left\{\varphi = \left(\varphi_1, \varphi_2, ..., \varphi_n\right) : \varphi \in \mathbb{C}\left(\left[-\upsilon, 0\right], \mathbb{R}^n_{+0}\right)\right\}$ *is the invariant domain of the following equation.*

$$\frac{dq_i\left(t\right)}{dt} = f_i\left(t, X_t\right), t \geq \sigma, i = 1, 2, ..., n. \tag{11}$$

Where

$$\mathbb{R}^{n}_{+0}\left\{\left(q_1,q_2,...,q_n\right): q_i \geq 0, i=1,2,...,n\right\} \tag{12}$$

Preposition 3.1. *The system* (1) *is invariant in* $\mathbb{R}^3_+$.

Proof: From system (1), we have:

$$\frac{dX}{dt} = P\left(X\left(t\right)\right), X\left(0\right) = X_0 \geq 0, \tag{13}$$

$$P\left(X(t)\right) = \left(P_1\left(X\right), P_2\left(X\right), P_3\left(X\right), P_4\left(X\right)\right)^T. \tag{14}$$

We noted that

$$\left.\begin{aligned} \left.\frac{dS\left(t\right)}{dt}\right|_{S=0} &= \Lambda \geq 0 \\ \left.\frac{dI\left(t\right)}{dt}\right|_{I=0} &= \frac{\mu SI}{S+R} \geq 0 \\ \left.\frac{dR\left(t\right)}{dt}\right|_{R=0} &= \kappa I \geq 0 \end{aligned}\right\}, \tag{15}$$

$\mathbb{R}^3_+$ is an invariant set, as stated by Lemma 3.1.

Preposition 3.2. *The system* (1) *is bounded in the region*

$$\Phi = \left\{\left(S\left(t\right), I\left(t\right), R\left(t\right)\right) \in \mathbb{R}^3 : N(t) \leq \frac{\Lambda}{\lambda}\right\}. \tag{16}$$

Proof: The sum of all equations in system (1) may be used to establish the boundedness of problem (1): Equation (16) has the following solution:

$$N\left(t\right) = \Lambda - \lambda N\left(t\right),$$

We get the solution:

$$N\left(t\right) \leq N_0 e^{-\lambda t} + \frac{\Lambda}{\lambda}\left(1 - e^{-\lambda t}\right). \tag{17}$$

As $t \to \infty$ then $N(t) \leq \frac{\Lambda}{\lambda}$. This indicates that the following is the feasible region for the given model:

$$\Phi = \left\{\left(S\left(t\right), I\left(t\right), R\left(t\right)\right) \in \mathbb{R}^3 : N(t) \leq \frac{\Lambda}{\lambda}\right\}. \tag{18}$$

As a result, the solution to system (1) is bounded.

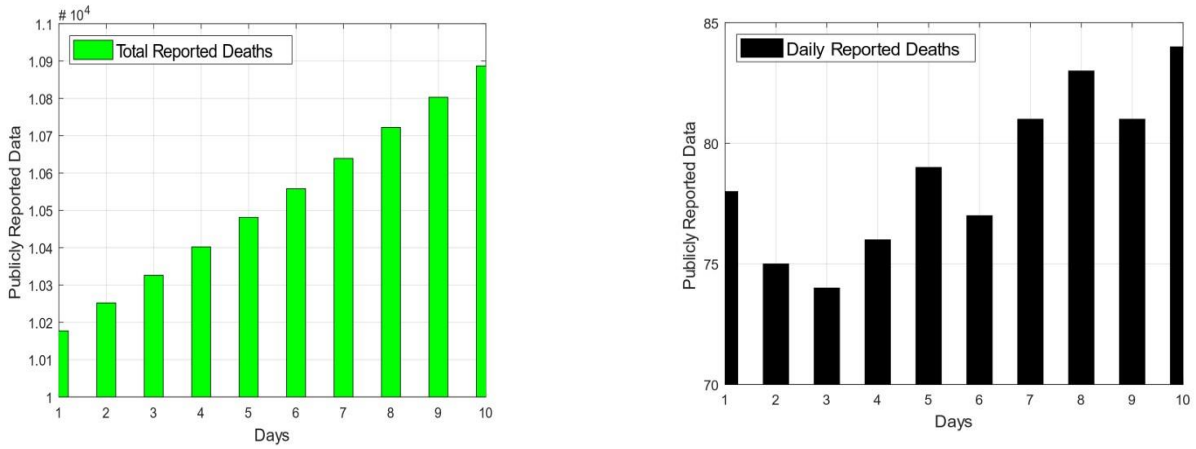

Figure 3. COVID-19-related fatalities reported to the public from October 30th to November 8th, 2020.

6. Fractional model and Numerical Scheme

6.2 : Preliminaries:

Definition 6.2.1: The time-fractional derivative of Atangana-Baleanu (AB) with fractional order γ is defined as [27].

$$ {}^{ABC}_{a}\wp^{\gamma}_{t} f(t) = \frac{\vartheta(\gamma)}{1-\gamma}\int_{a}^{\tau} E_{\gamma}\left(\frac{-\gamma(\tau-t)^{\gamma}}{1-\gamma}\right) f'(\tau)\,dt, \text{ for } \; 0<\gamma<1. \tag{19} $$

Here, $\vartheta(\gamma)$ is the normalization function and $E_{\gamma}(.)$ is the Mittage-Leffler function [28].

Definition 6.2.2: Consider a non-linear fractional ODE:

$$ {}^{ABC}\wp^{\gamma}_{t} y(t) = f(t, y(t)) \;\text{ with }\; y(0) = y_0, \tag{20} $$

Equation (23) has the following numerical scheme [29]:

$$y_{w+1}=y_0+\frac{1-\gamma}{\mathcal{G}(\gamma)}f\left(t_w,y(t_w)\right)+\frac{\gamma}{\mathcal{G}(\gamma)}\sum_{m=0}^{w}\left[\begin{array}{l}\dfrac{h^\gamma f\left(t_m,y(t_m)\right)}{\Gamma(\gamma+2)}\left\{(w+1-m)^\gamma(w+2-m+\gamma)-(w-m)^\gamma(w+2-m+2\gamma)\right\}\\ -\dfrac{h^\gamma f\left(t_{m-1},y(t_{m-1})\right)}{\Gamma(\gamma+2)}\left\{(w+1-m)^{\gamma+1}-(w-m)^\gamma(w+1-m+\gamma)\right\}\end{array}\right]. \tag{21}$$

6.3 Fractional model:

By utilizing the Atangana-Baleanu time-fractional operator, we get:

$$\left.\begin{array}{l}{}^{ABC}\wp_t^\gamma S(t)=\Lambda-\lambda S-\dfrac{\mu SI}{N},\\ {}^{ABC}\wp_t^\gamma I(t)=\dfrac{\mu SI}{N}-\lambda I-\kappa I,\\ {}^{ABC}\wp_t^\gamma R(t)=\kappa I-\lambda R,\end{array}\right\} \tag{22}$$

Here, γ is fractional parameter and ${}^{ABC}_{0}\wp_t^\gamma(.)$ AB time fractional operator.

6.4 Numerical Scheme:

Model (22) takes the following suitable form when using the procedure in [29]:

$$\left.\begin{array}{l}{}^{ABC}\wp_t^\gamma S(t)=\psi_1(t,S,I,R),\\ {}^{ABC}\wp_t^\gamma I(t)=\psi_2(t,S,I,R),\\ {}^{ABC}\wp_t^\gamma R(t)=\psi_3(t,S,I,R),\end{array}\right\} \tag{23}$$

We get the following iterative form:

$$S(t_{w+1})=S(t_0)+\frac{1-\gamma}{\mathcal{G}(\gamma)}\psi_1\left(t_w,S_w(t)\right)+\frac{\gamma}{\mathcal{G}(\gamma)}\sum_{z=0}^{w}\left[\begin{array}{l}\dfrac{h^\gamma\psi_1\left(t_z,S(t_z)\right)}{\Gamma(\gamma+2)}\left\{(w+1-z)^\gamma(k+2-z+\gamma)-(w-z)^\gamma(w+2-z+2\gamma)\right\}\\ -\dfrac{h^\gamma\psi_1\left(t_{z-1},S(t_{z-1})\right)}{\Gamma(\gamma+2)}\left\{(w+1-z)^{\gamma+1}-(w-z)^\gamma(w+1-z+\gamma)\right\}\end{array}\right], \tag{33}$$

$$I\left(t_{w+1}\right)=I\left(t_0\right)+\frac{1-\gamma}{\vartheta(\gamma)}\psi_2\left(t_w,I_w\left(t\right)\right)$$
$$+\frac{\gamma}{\vartheta(\gamma)}\sum_{z=0}^{w}\left[\begin{array}{l}\dfrac{h^{\gamma}\psi_2\left(t_z,I\left(t_z\right)\right)}{\Gamma(\gamma+2)}\left\{\left(w+1-z\right)^{\gamma}\left(k+2-z+\gamma\right)-\left(w-z\right)^{\gamma}\left(w+2-z+2\gamma\right)\right\}\\ -\dfrac{h^{\gamma}\psi_2\left(t_{z-1},I\left(t_{z-1}\right)\right)}{\Gamma(\gamma+2)}\left\{\left(w+1-z\right)^{\gamma+1}-\left(w-z\right)^{\gamma}\left(w+1-z+\gamma\right)\right\}\end{array}\right], \tag{34}$$

$$R\left(t_{w+1}\right)=R\left(t_0\right)+\frac{1-\gamma}{\vartheta(\gamma)}\psi_3\left(t_w,R_w\left(t\right)\right)$$
$$+\frac{\gamma}{\vartheta(\gamma)}\sum_{z=0}^{w}\left[\begin{array}{l}\dfrac{h^{\gamma}\psi_3\left(t_z,R\left(t_z\right)\right)}{\Gamma(\gamma+2)}\left\{\left(w+1-z\right)^{\gamma}\left(k+2-z+\gamma\right)-\left(w-z\right)^{\gamma}\left(w+2-z+2\gamma\right)\right\}\\ -\dfrac{h^{\gamma}\psi_3\left(t_{z-1},R\left(t_{z-1}\right)\right)}{\Gamma(\gamma+2)}\left\{\left(w+1-z\right)^{\gamma+1}-\left(w-z\right)^{\gamma}\left(w+1-z+\gamma\right)\right\}\end{array}\right], \tag{35}$$

7. Data Fitting and Numerical Results

7.1 Data Fitting

Model (22) is fitted with real data by getting some parameter values from the literature and fitting or estimating the remaining values for data gathered during the time period under consideration. The model's solution is calibrated using real data from worldometer [30] for Turkey from October 30 to November 8, 2020. Turkey's overall population is estimated to be 84675323 people in 2020 [29]. The total population is considered as the total initial population i.e. $N\left(0\right)=84675323$ which is subcategorized into three different classes such that the infected class that is denoted by $I(0)$ and to be considered as $I(0)$=373154, the recovered or removed population is $R(0)$=dead+recovered=332652 and the remaining is considered as susceptible population $S(0)$=83969517. The values for the other parameters are portrayed in table 1. $\mathfrak{R}_0$ is estimated as $\mathfrak{R}_0\approx 1.09457$ for table 1 values.

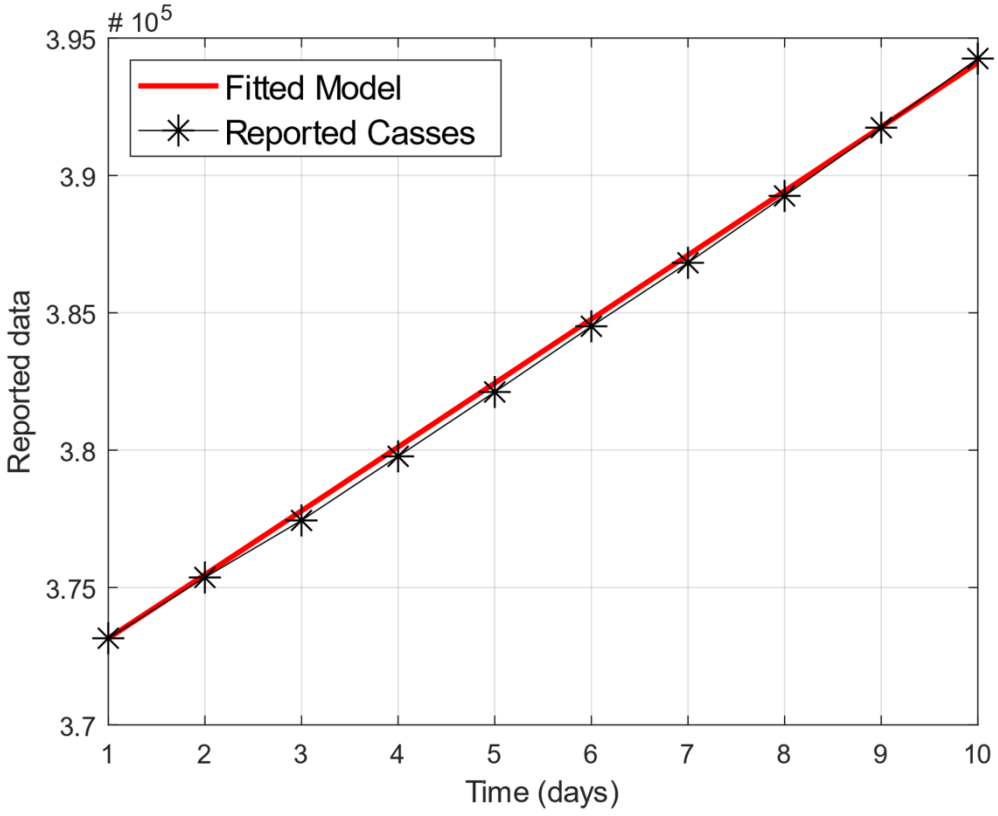

Figure 4. Real data verses model fitting.

Table 1. Model 1 estimated and fitted values for various parameters.

Parameter	Description	Value	Source
Λ	Birth rate	$\lambda \times N(0)$	Estimated
λ	Natural Mortality rate	$\frac{1}{78.45 \times 365}$	[31]
μ	Contact rate	0.07992	Fitted
κ	Recovery rate	0.07298	Fitted

7.2 Numerical Results:

This section of the article contains a variety of graphical results. The interaction between different compartments is seen in Figure 1. To forecast the transmission of COVID-19, it is critical to examine the virus's spread and the impact of these parameters. Figure 2 shows the publicly reported COVID-19 infected cases between October 30th and November 8th, 2020.

Figure 3 depicts the total number of deaths linked to COVID-19 throughout the relevant time period. The real data vs model fitting is seen in Figure 4. The graph shows that our model agrees well with real-world data. Moreover, the numerical results of the present model are calculated through a numerical scheme by using the computational software MATLAB. The time interval is considered in days. It is important to discuss here that the considered period is the most recent data, and we believe that it will give the current situation of COVID-19 in Turkey more precisely, and it will also give us more accurate predictions for the transmission of the disease.

The COVID-19 spread in various classes are shown in Figure 5 using fixed values from Table 1. The impact of the fractional parameter γ on different compartments is seen in Figure 6. The obtained solutions provide interesting findings and provide a range of results to the present model by changing γ while keeping other variables constant. We can see from the graph that raising γ reduces infected people and delays the time it takes to reach the maximum number in each compartment. With the exception of the susceptible class, decreasing γ flattens the curves of all population compartments. The influence of contact rate μ on different classes is portrayed in figure 7. By increasing μ, susceptible individuals rapidly decrease and entered in the infected class which increases the number of infected individuals and then entered to the recovered class from the infected class by some means of recovery rate. Figure 8 displays the impact of the recovery rate κ on the number of individuals in different compartments. From the figure, it can be seen that by increasing κ increases the number of susceptible individuals and the same behavior of κ can be also seen for the infected and recovered classes. This behavior of κ is obvious because when we increase the recovery rate then the infected individuals will become quickly recover and will enter rapidly in the recovered class. If the infected individuals decreases, then the contact among the susceptible and infected individuals will be decreased because there will be not enough infected individuals to interact with the susceptible ones and in this way less people will get infected. Similarly, if fewer people get infected, then there will not be enough people remains in the infected class to recover and in this way the recovered class will be decreases. Furthermore, all of the figures show that we have forecasted COVID-19 dynamics and transmission in Turkey for the next 800 days. Figure 9 shows the global asymptotical stability of the current model when various initial values are taken into account. Finally, the vaiation of $\Re_0$ against μ and κ is presented in figure 10. It is noticed that the interaction rate μ increases $\Re_0$ while a decrease is noticed for large values of recovery rate κ.

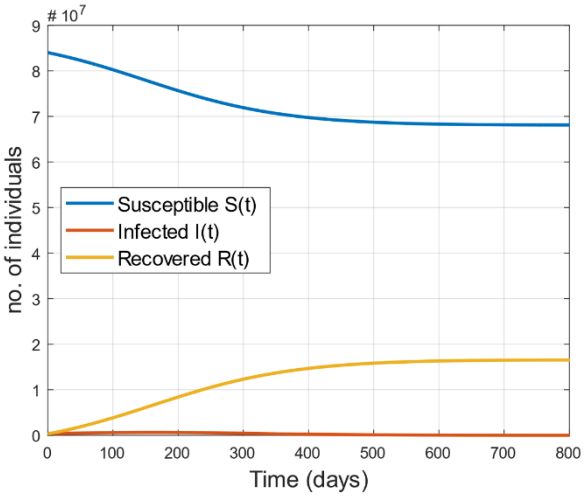

Figure 5: Dynamics of COVID-19 in different classes for fixed values.

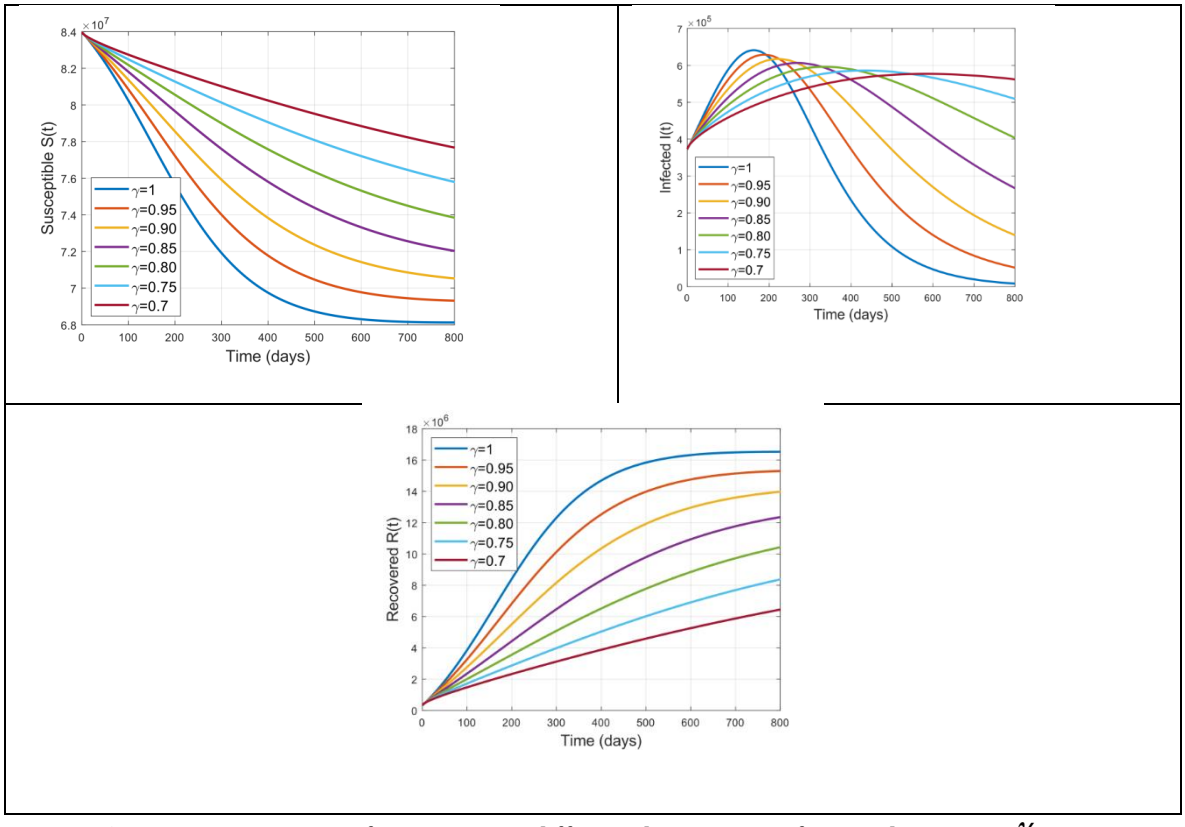

Figure 6. Transmission of COVID-19 in different classes against fractional parameter γ .

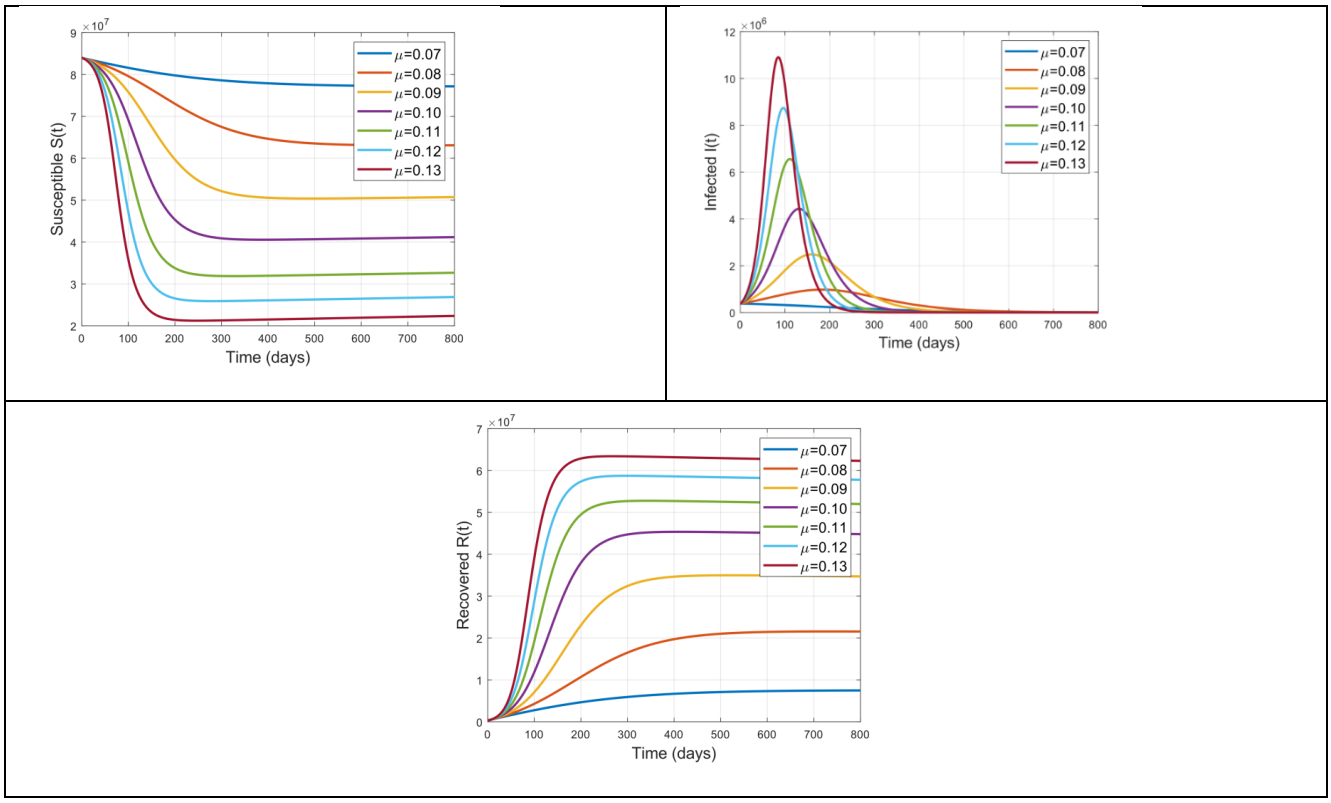

Figure 7. Transmission of COVID-19 in different classes against contact rate μ.

8. Concluding Remarks:

The SIR model for COVID-19 transmission in Turkey has been explored in this paper. The model is both bounded and invariant, as we've demonstrated. Two equilibrium points, DFE and EE, are computed for the steady-state of the proposed model. In addition, the reproduction number is calculated. We've also used the recently developed AB fractional operator to the classic SIR model, which has been generalized. The real data was fitted to the classical model $(\gamma = 1)$ using the data. The basic reproduction number has been estimated using the fitted values in table 1 as $\Re_0 \approx 1.09457$. Different graphical results have been produced after simulation of the numerical method. We've examined at days as a unit of time. Furthermore, COVID-19's behaviours are predicted for the following 800 days. By reducing the values of the fractional parameter γ, a decline in the infected class is seen. An increase in infected class and decrease in susceptible class is observed by increasing the contact rate μ. The opposite behavior for recovery rate κ is noticed in susceptible and infected compartments. If we try to decrease the interaction between the people by taking some proper measurements then the infection will die out more quickly with less loss of individuals. Similarly, if we increase the recovery rate κ by introducing some proper treatment or

vaccination, then the infection will die out from the population without great loss. Because infectious diseases are still uncontrollable on a global level. We are all aware that scientists and researchers are working to develop a good medical therapy or vaccine to prevent the development of COVID-19. In the future, the quarantine or vaccine categories, or both, might be added to the model to demonstrate how these classes affect the spread of this fatal acute disease. One can also add some control parameters in the present problem to show the effect of different controls such as isolation, vaccination or quarantine, etc.

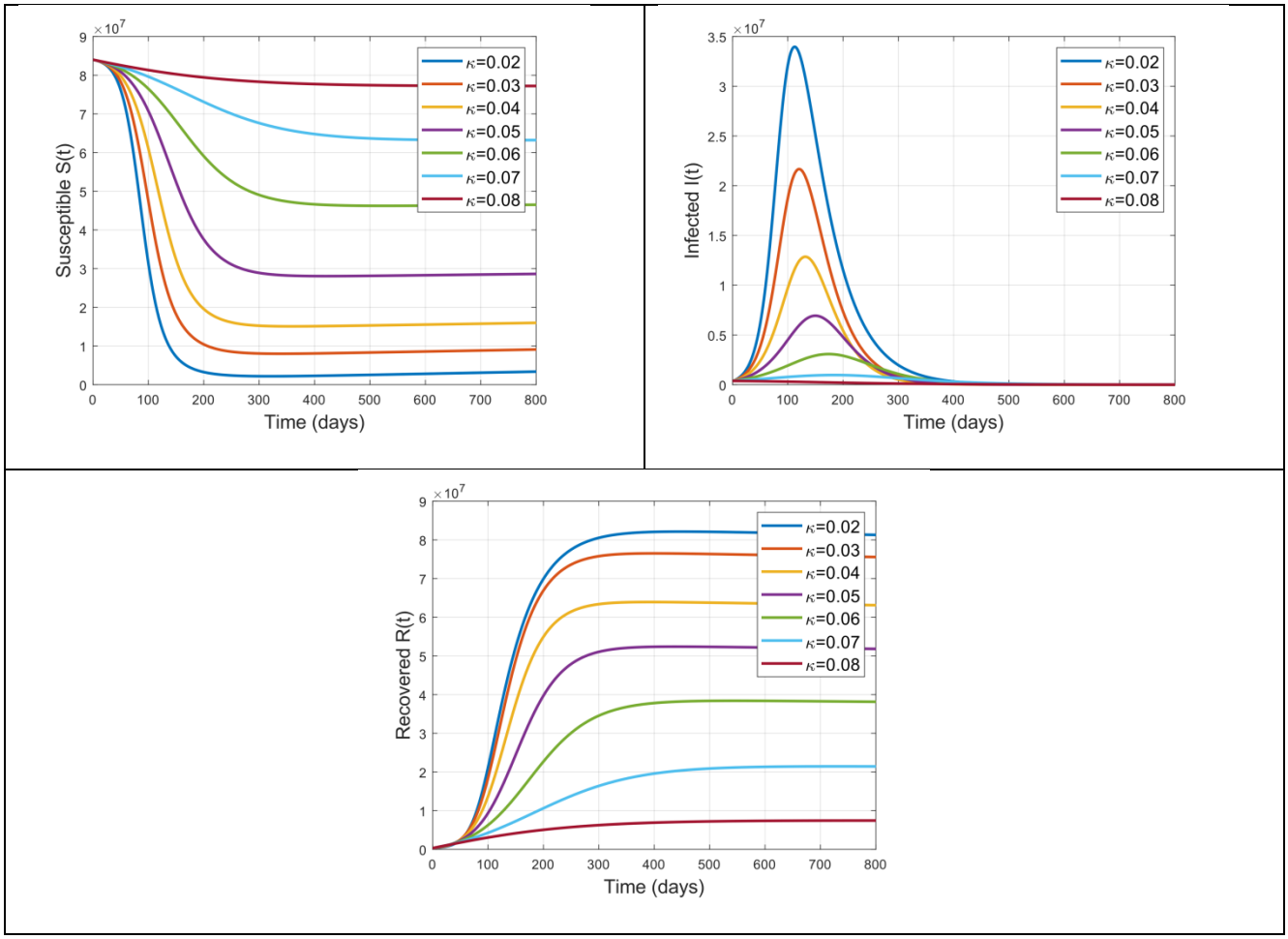

Figure 8. Transmission of COVID-19 in different classes against recovery rate κ.

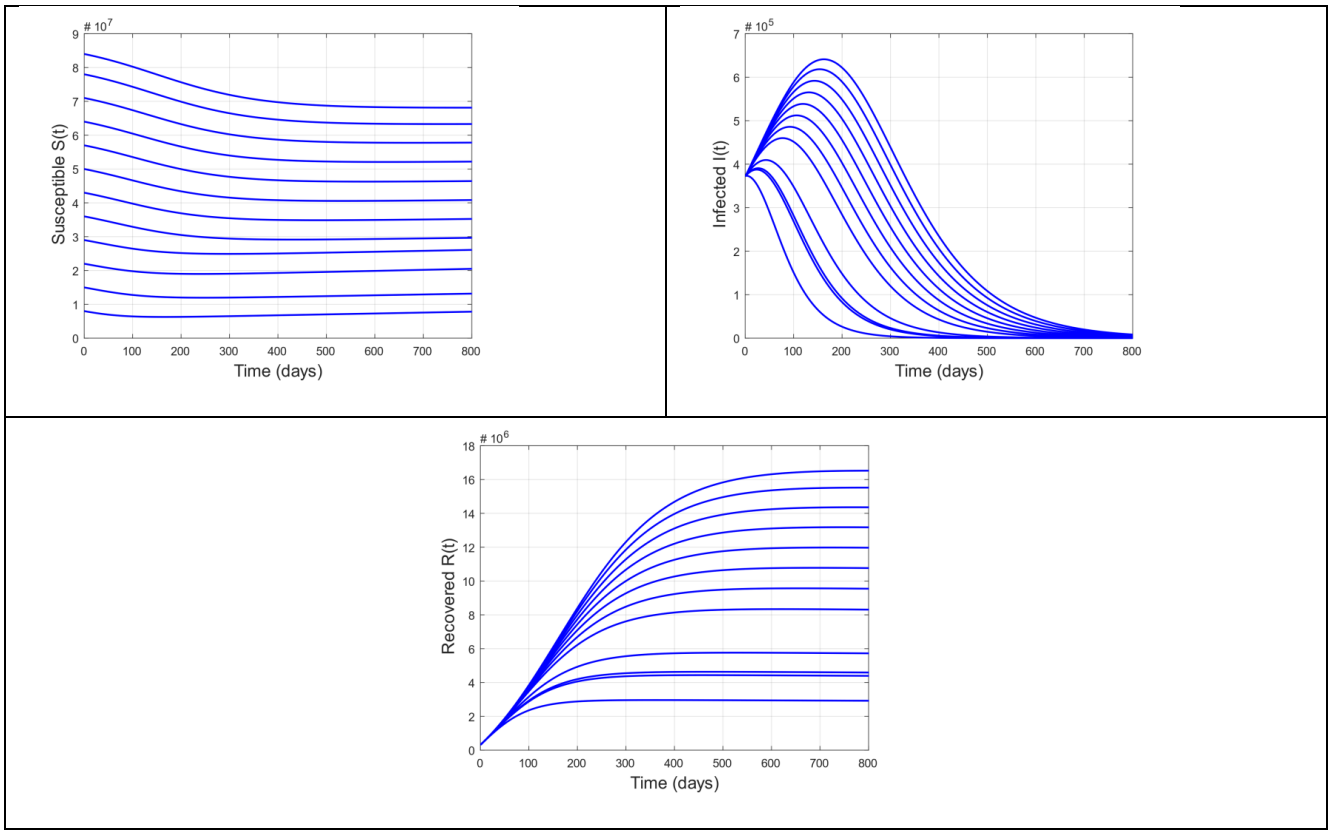

Figure 9. COVID-19 dynamics in various classes with various initial conditions.

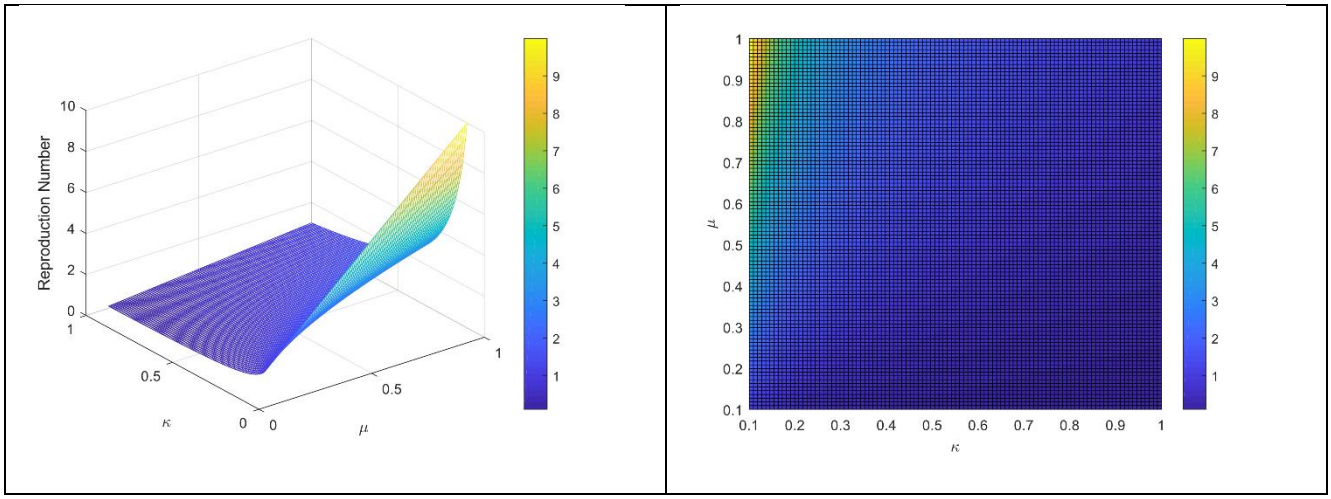

Figure 10. Variation in Reproduction number against interation and recovery rates.

Acknowledgement

The authors are extremely grateful to ORIC-CUSIT for their great assistance and resources in carrying out this research. The authors are also grateful to CUSIT's Department of Health Sciences for providing them with real data.

References

[1] Fan, Y., Zhao, K., Shi, Z. L., & Zhou, P. (2019). Bat coronaviruses in China. *Viruses*, *11*(3), 210.

[2] World Health Organization. Coronavirus disease 2019 (COVID-19): situation report, **73** https://apps.who.int/iris/handle/10665/331686 (2020).

[3] Zhang Y, Chen C, Zhu S et al. [Isolation of 2019-nCoV from a stool specimen of a laboratory-confirmed case of the coronavirus disease 2019 (COVID-19)]. China CDC Weekly;2(8):1234. (In Chinese). 2020.

[4] Liu Y, Cui J. The impact of media coverage on the dynamics of infectious diseases. Int J Biomath 2008;1(1):65–74.

[5] Zou, L. et al. (2020). SARS-CoV-2 viral load in upper respiratory specimens of infected patients. N. Engl. J. Med. Published online February 19, 2020.

[6] Zhu, N. et al. (2020). A novel coronavirus from patients with pneumonia in China, N. Engl. J. Med. 382, 2019, 727-733.

[7] Senel, K., Ozdinc, M., & Ozturkcan, S. (2020). Single Parameter Estimation Approach for Robust Estimation of SIR Model With Limited and Noisy Data: The Case for COVID-19. *Disaster Medicine and Public Health Preparedness*, 1-15.

[8] Chen, Y. C., Lu, P. E., Chang, C. S., & Liu, T. H. (2020). A Time-dependent SIR model for COVID-19 with undetectable infected persons. *IEEE Transactions on Network Science and Engineering*.

[9] Cooper, I., Mondal, A., & Antonopoulos, C. G. (2020). A SIR model assumption for the spread of COVID-19 in different communities. *Chaos, Solitons & Fractals*, *139*, 110057.

[10] Simha, A., Prasad, R. V., & Narayana, S. (2020). A simple stochastic sir model for covid 19 infection dynamics for karnataka: Learning from europe. *arXiv preprint arXiv:2003.11920*.

[11] Lai, J., Mao, S., Qiu, J., Fan, H., Zhang, Q., Hu, Z., & Chen, J. (2016). Investigation progresses and applications of fractional derivative model in geotechnical engineering. *Mathematical Problems in Engineering*, *2016*.

[12] Ali, F., Ahmad, Z., Arif, M., Khan, I., & Nisar, K. S. (2020). A Time Fractional Model of Generalized Couette Flow of Couple Stress Nanofluid With Heat and Mass Transfer: Applications in Engine Oil. *IEEE Access*, *8*, 146944-146966.

[13] Arif, M., Ali, F., Khan, I., & Nisar, K. S. (2020). A Time Fractional Model With Non-Singular Kernel the Generalized Couette Flow of Couple Stress Nanofluid. *IEEE Access*, *8*, 77378-77395.

[14] Akgül, A., & Khoshnaw, S. A. (2020). Application of fractional derivative on non-linear biochemical reaction models. *International Journal of Intelligent Networks*, *1*, 52-58.

[15] Rajagopal, K., Hasanzadeh, N., Parastesh, F., Hamarash, I. I., Jafari, S., & Hussain, I. (2020). A fractional-order model for the novel coronavirus (COVID-19) outbreak. *Nonlinear Dynamics*, *101*(1), 711-718.

[16] Alkahtani, B. S. T., & Alzaid, S. S. (2020). A novel mathematics model of covid-19 with fractional derivative. Stability and numerical analysis. *Chaos, Solitons & Fractals*, *138*, 110006.

[17] Yadav, R. P., & Verma, R. (2020). A numerical simulation of fractional order mathematical modeling of COVID-19 disease in case of Wuhan China. *Chaos, Solitons & Fractals*, *140*, 110124.

[18] Qureshi, S., & Yusuf, A. (2019). Fractional derivatives applied to MSEIR problems: Comparative study with real world data. *The European Physical Journal Plus*, *134*(4), 171.

[19] Qureshi, S., & Atangana, A. (2019). Mathematical analysis of dengue fever outbreak by novel fractional operators with field data. *Physica A: Statistical Mechanics and its Applications*, *526*, 121127.

[20] Abdo, M. S., Shah, K., Wahash, H. A., & Panchal, S. K. (2020). On a comprehensive model of the novel coronavirus (COVID-19) under Mittag-Leffler derivative. *Chaos, Solitons & Fractals*, 109867.

[21] Ahmad, Z., Arif, M., Ali, F., Khan, I., & Nisar, K. S. (2020). A report on COVID-19 epidemic in Pakistan using SEIR fractional model. *Scientific Reports*, *10*(1), 1-14.

[22] Sheikh, N. A., Ali, F., Saqib, M., Khan, I., Jan, S. A. A., Alshomrani, A. S., & Alghamdi, M. S. (2017). Comparison and analysis of the Atangana–Baleanu and Caputo–Fabrizio fractional derivatives for generalized Casson fluid model with heat generation and chemical reaction. *Results in physics*, *7*, 789-800.

[23] Ghanbari, B., Günerhan, H., & Srivastava, H. M. (2020). An application of the Atangana-Baleanu fractional derivative in mathematical biology: A three-species predator-prey model. *Chaos, Solitons & Fractals*, *138*, 109910.

[24] Sheikh, N. A., Ali, F., Khan, I., Gohar, M., & Saqib, M. (2017). On the applications of nanofluids to enhance the performance of solar collectors: A comparative analysis of Atangana-Baleanu and Caputo-Fabrizio fractional models. *The European Physical Journal Plus*, *132*(12), 540.

[25] Ali, F., Khan, I., Sheikh, N. A., & Gohar, M. (2019). Exact solutions for the Atangana-Baleanu time-fractional model of a Brinkman-type nanofluid in a rotating frame: Applications in solar collectors. *The European Physical Journal Plus*, *134*(3), 1-18.

[26] Murtaza, S., Farhad Ali, A., Sheikh, N. A., Khan, I., & Nisar, K. S. (2020). Exact Analysis of Non-Linear Fractionalized Jeffrey Fluid. A Novel Approach of Atangana-Baleanu Fractional Model. *CMC-COMPUTERS MATERIALS & CONTINUA*, *65*(3), 2033-2047.

[27] Atangana, A., & Baleanu, D. New fractional derivatives with non-local and non-singular kernel: theory and application to heat transfer model. *arXiv preprint* arXiv:1602.03408 (2016).

[28] Sene, N. SIR epidemic model with Mittag–Leffler fractional derivative. *Chaos, Solitons & Fractals*, **137**, 109833 https://doi.org/10.1016/j.chaos.2020.109833 (2020).

[29] Toufik, M., & Atangana, A. New numerical approximation of fractional derivative with non-local and non-singular kernel: application to chaotic models. *The European Physical Journal Plus*, **132**, 444 https://doi.org/10.1140/epjp/i2017-11717-0 (2017).

[30] COVID-19 situation in Turkey, https://www.worldometers.info/coronavirus/country/-turkey.

[31] Population of Turkey, https://www.worldometers.info/world-population/turkey-population.

[32] Life expectancy in Turkey, https://www.worldlifeexpectancy.com/turkey-life-expectancy